Journal of Structural Geology, Vol. 14, No. 10, pp. 1253 to 1266, 1992
Printed in Great Britain

0191-8141/92 $05.00+0.00

Mechanical interactions between rigid particles in a deforming ductile matrix. Analogue experiments in simple shear flow

BENOÎT ILDEFONSE*

Geologisches Institut, ETH-Zentrum, CH-8092 Zürich, Switzerland

DIMITRIOS SOKOUTIS

The Hans Ramberg Tectonic Laboratory, Institute of Geology, Uppsala University, Box 555, S-75122 Uppsala, Sweden

and

NEIL S. MANCKTELOW

Geologisches Institut, ETH-Zentrum, CH-8092 Zürich, Switzerland

(*Received* 25 *July* 1991; *accepted in revised form* 1 *May* 1992)

Abstract—The mechanical interaction between two or more particles is investigated in Newtonian simple shear flow. The experimental models allow observation of both the particle rotation and the deformation pattern around the particles. The finite and instantaneous strain patterns around rigid particles are strongly heterogeneous and asymmetric, with high finite strain zones aligned to the direction of maximum finite stretch. These correspond to local flow with low vorticity number. Heterogeneous strain patterns around rigid particles spread over a distance of 1–2 times the particle length and this distance increases with increasing bulk strain. Where rigid particles are more concentrated, these patterns coalesce and the overall pattern is then strongly controlled by the particles and cannot be simply related to the external boundary conditions. In rocks, the characteristic asymmetric strain pattern around rigid isolated particles is a reliable shear criterion, which becomes unreliable with high concentrations of rigid particles. Particle rotation is significantly disturbed when the distance between adjacent particles of equal size is shorter than their length, that is only in very concentrated suspensions of rigid particles. In a composite shape fabric, the development of the sub-fabric corresponding to the smaller minerals will be more disturbed.

INTRODUCTION

NUMEROUS structures in rocks, such as boudins (Goguel 1948, Lloyd & Ferguson 1981, Goldstein 1988, Malavieille & Lacassin 1988), porphyroclasts (Passchier & Simpson 1986, Passchier 1987, Van Den Driessche & Brun 1987) and shape preferred orientations (Blumenfeld & Bouchez 1988, Fernandez 1988, Benn & Allard 1989, Ildefonse *et al.* 1990) result from progressive deformation of a system composed of rigid particles distributed in a ductile matrix. The form and symmetry of these structures are commonly used as tools for structural and kinematic analysis. Methods used to analyse such structures are based on the simple model of Jeffery (1922), which considers the rotation of an isolated axisymmetric ellipsoidal rigid particle in a Newtonian fluid (e.g. Jeffery 1922, Ramsay 1967, pp. 221–226, Gay 1968, Reed & Tryggvason 1974, Ghosh & Ramberg 1976, Fernandez *et al.* 1983, Passchier 1987). However, natural structures are quite frequently controlled by rigid particle populations sufficiently concentrated to produce contact between at least some of the particles. The resulting particle tiling is currently used as shear criterion in magmatic rocks (Den Tex 1969, Blanchard *et al.* 1979, Blumenfeld & Bouchez 1988). Except for this important application, the disturbance in particles' behaviour, which results from interference between neighbours, has been largely neglected. The more detailed effects of mechanical interactions between rigid objects in rocks has not been fully investigated because no analytical solution to this problem has yet been developed. We must, therefore, rely on experimental or numerical modelling in order to integrate these effects into methods for structural and kinematic analysis of rigid particle fabrics.

An earlier series of experiments (Ildefonse & Fernandez 1988, Ildefonse *et al.* 1992) clearly demonstrated the influence, in two dimensions, of the concentration of particles on the development of a shape preferred orientation. Interactions between particles were responsible for a decrease in the fabric intensity and, in simple shear flow, for a perturbation in the cyclic rotation of the fabric axis (Ildefonse *et al.* 1992). It was suggested that the changing velocity of particle rotation was due not only to actual collision between particles, but also to

*Present address: Laboratoire de Tectonophysique, Université Montpellier II, 34095, Montpellier Cédex 05, France.

perturbation in the matrix flow around closely-spaced neighbours. It was emphasized, however, that the limiting distance, below which particles significantly interact, was not well established. Anczurowski *et al.* (1967), studying the behaviour of rigid rods in a fluid subjected to couette flow considered that "the effect of particle collisions are important however dilute the suspension may be, provided that it is sheared for a sufficiently long time". In geology, however, we are dealing with only limited finite shear strains. Burgers (1938) suggested that in a liquid in laminar motion "every particle should dispose of a volume which is large compared with the third power of its length". This would imply that interactions have non-negligible effects on the development of most natural rigid particle fabrics found in geology.

The experimental work presented here was performed to obtain a more detailed understanding of the mechanical interaction between two or more particles in simple shear flow. The analogue models, more simple than earlier models, allow an investigation of particle rotation as a function of the distance between adjacent particles and of the initiation and development of the heterogeneous strain field around the particles.

METHOD

The models were run in the Hans Ramberg Tectonic Laboratory of the Uppsala University, using a simple shear box composed of 100 U-shape metal plates, each 1 mm thick (Fig. 1). Each plate is free to move relative to others, the sides of the box perpendicular to the plates being constrained by two rotating plates. Homogeneous simple shear in the model (in the central part of the box, within the 'U' region of the plates) is achieved by pulling the last plate of the set, this movement being generated by an electric motor (Fig. 1). The upper surface of the model is unconstrained. Local changes in surface area (determined from analysis of the inscribed grid, see below) remain small for all the experiments, demonstrating a close approximation to plane strain.

The material used as a ductile matrix was a Newtonian silicone bouncing putty 'Rhodorsil Gomme GSIR', supplied by Rhône Poulenc (Paris) (see Sokoutis 1987 for calibration). Particles were blocks of Plexiglas with an aspect ratio of 3 (18 mm long, 6 mm wide and 40 mm thick) floating in the silicone putty. A passive grid made of carbon powder covers the model surface, allowing an analysis of the progressive deformation field. The fine carbon grids were produced according to the 'photocopy' method of Dixon & Summers (1985, p. 93), with a modification in that it proved more useful to use transparent (acetate) sheets, rather than paper (Treagus & Sokoutis 1992). There is perfect coherence across the particle–matrix interface, as demonstrated by the lack of any offset in marker lines. The applied constant shear strain rate was $2 \pm 0.4 \times 10^{-3}\ s^{-1}$ (corresponding to a natural strain rate of $1 \pm 0.2 \times 10^{-3}\ s^{-1}$).

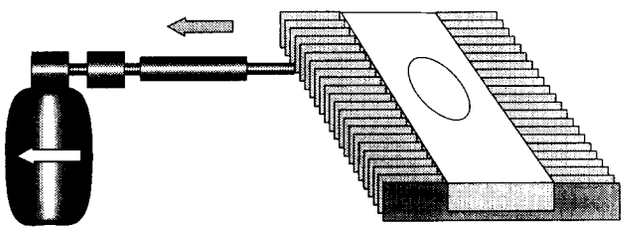

Fig. 1. Schematic drawing of the shear box at the Hans Ramberg Tectonic Laboratory at Uppsala (Sweden), seen after shearing. The sense of shear is sinistral.

A sequence of photographs were taken on each run and enlarged prints were subsequently digitized. From this successive record of the grid inscribed on the top of the models, the progressive displacement and deformation history around the rigid particles could be determined. Calculations based on the digitized position of grid nodes were computed using a Macintosh menu-driven program (Mancktelow 1991). The orientation of the particles has been manually measured directly from the photographs.

EXPERIMENTAL RESULTS

Perturbation around the particles

The most immediate result obtained from this type of experiment (e.g. Ghosh 1975, Ghosh & Ramberg 1976, Van Den Driessche & Brun 1987) is the heterogeneous deformation field developed around the particles (Fig. 2). The perturbation induced by the presence of the rigid particle is easily envisaged by partitioning the overall deformation into homogeneous and heterogeneous components (Mancktelow 1991). The perturbation in the finite displacement is graphically represented by plotting the vectors joining the nodes of the grid corresponding to the homogeneous component to the actual grid (Fig. 3). These 'perturbation vectors', distributed as closed loops around the particles, show that the perturbation in the displacement field extends to a large distance (minimum 1–2 times the particle length) away from each rigid particle. The higher the bulk finite strain, the larger the zone of perturbation around the particle. In all runs presented here (except run 10), the particles are close enough for these disturbed zones to coalesce at $\gamma = 0.8$.

Finite strain pattern

As a consequence of the perturbation induced by the rigid particles, the local finite strain field is highly heterogeneous, both in orientation of the principal axes of finite strain (Fig. 4) and finite strain magnitude (Fig. 5). In all runs except run 6, the particles are oriented oblique to the passive grid lines (Fig. 2). As a result, the few strain magnitudes calculated across the particle–matrix interface are non-significant and represent an average over a discontinuity in strain values. At $\gamma = 0.8$, the normal background natural finite strain is 0.39 (sinh $\varepsilon = \gamma/2$, Hsu 1966). Contour values of 0.35 and 0.5 (0.45

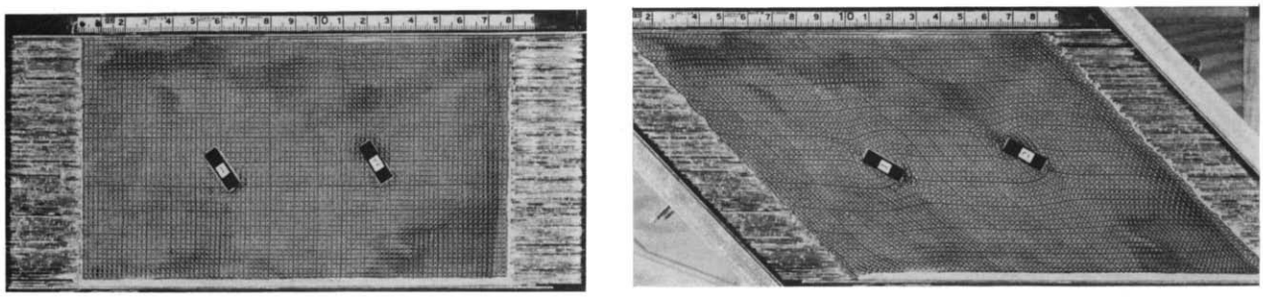

Run 10

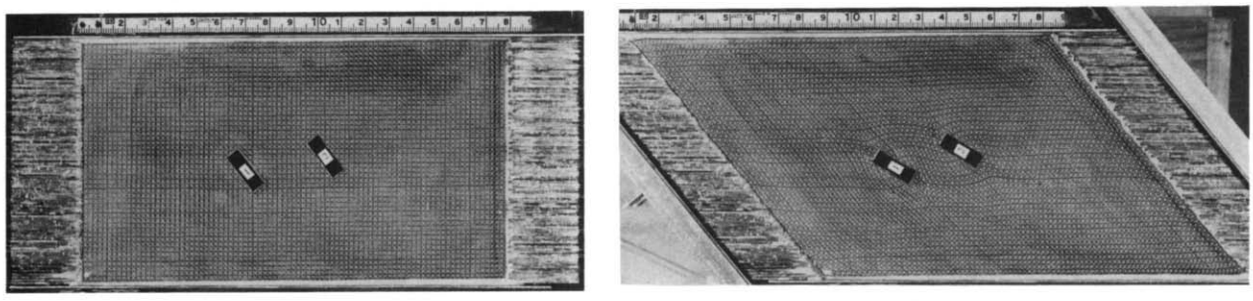

Run 11

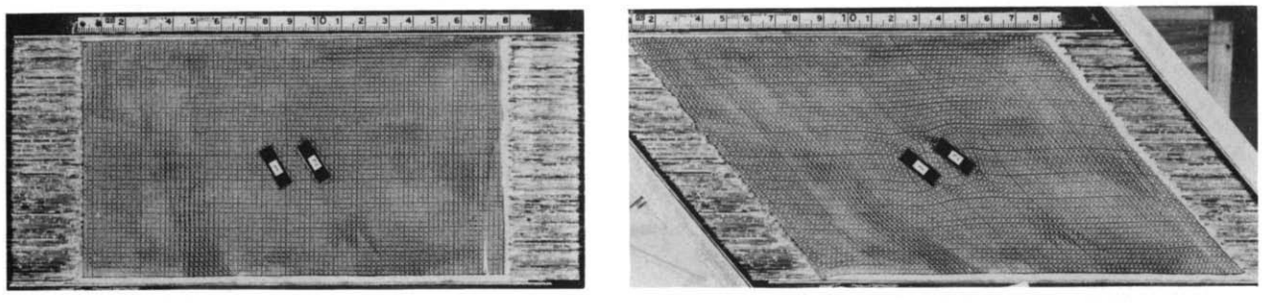

Run 12

Fig. 2. Initial and deformed ($\gamma \approx 0.8$) stages of runs 10, 11, 12, 6, 13 and 15. In all runs, the grid is initially a set of vertical and horizontal lines.

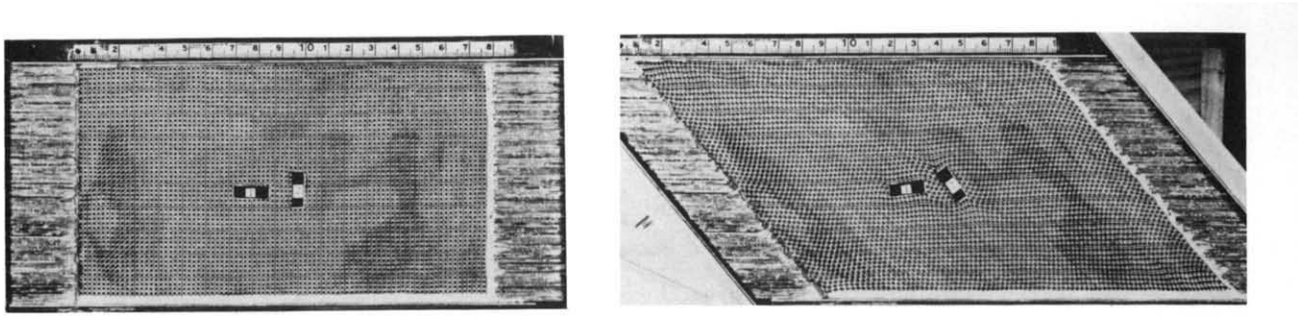

Run 6

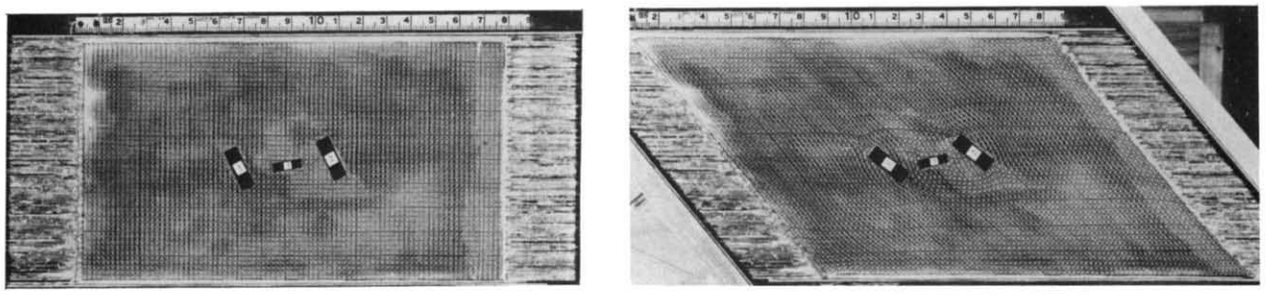

Run 13

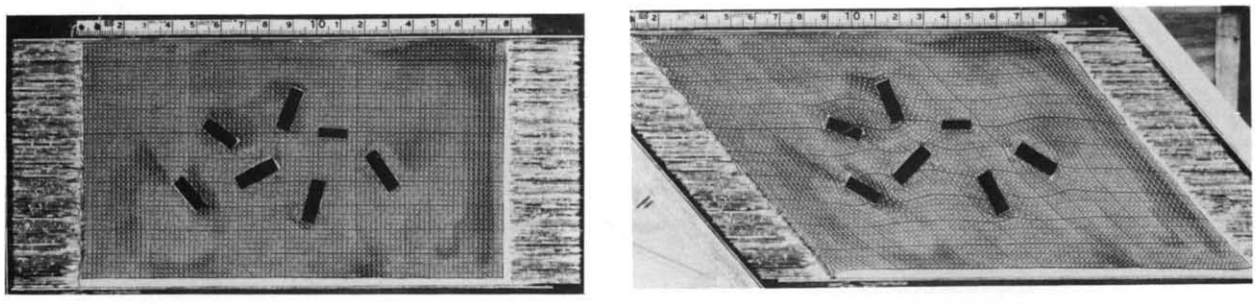

Run 15

Fig. 2. *Continued.*

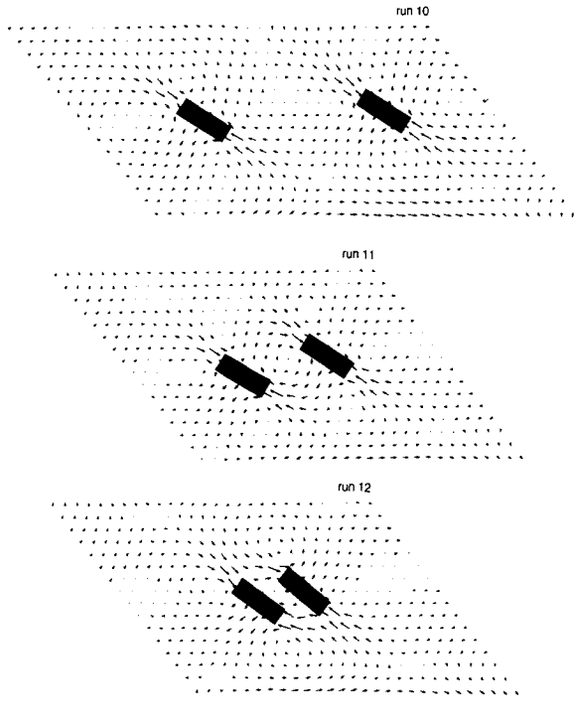

Fig. 3. Perturbation induced by the particles in runs 10, 11 and 12. Perturbation is visualized by the vectors join the nodes of the homogeneous background simple shear grid (obtained from best-fit calculation; see Mancktelow 1991) to the nodes of the model grid.

in run 6) were chosen to bound the area where the finite strain field is not disturbed, or only slightly so. When the particle is far enough from its neighbour to behave as if it were completely isolated (run 10), the surrounding strain field shows an asymmetric pattern with two major high strain zones, aligned along the bulk finite strain major axis (34.1° for $\gamma = 0.8$), bounded by four low strain ones (Fig. 5). Similar patterns are observed in half-sectors unaffected by interactions (left and right sides of the models) in runs 11, 12, 13 and 6. It is slightly different on the left side in run 6, where the particle is initially lying sub-parallel to the shear plane; two additional small high strain zones appear, while low strain is reduced to one zone on each side of the particle. When particles are close enough for interaction to occur (centre part in runs 11, 12, 13, 6 and run 15), this pattern is obviously changed. The strain field is then locally strongly controlled by the spacing and orientation of the rigid particles (see below).

Instantaneous deformation pattern

In order to describe the instantaneous deformation pattern which is responsible for the observed finite strain pattern, we use the kinematic vorticity number W_k (Truesdell 1953, McKenzie 1979, Means *et al.* 1980, Passchier 1986, Mancktelow 1991). This number is, at a given point, the ratio between the magnitude of the vorticity vector (the vorticity is the antisymmetric component of the velocity gradient tensor) and an invariant term related to the eigenvalues of the rate-of-deformation tensor (symmetric component of the velocity gradient tensor). More simply, relative to an arbitrary fixed reference frame (Truesdell 1953, Passchier

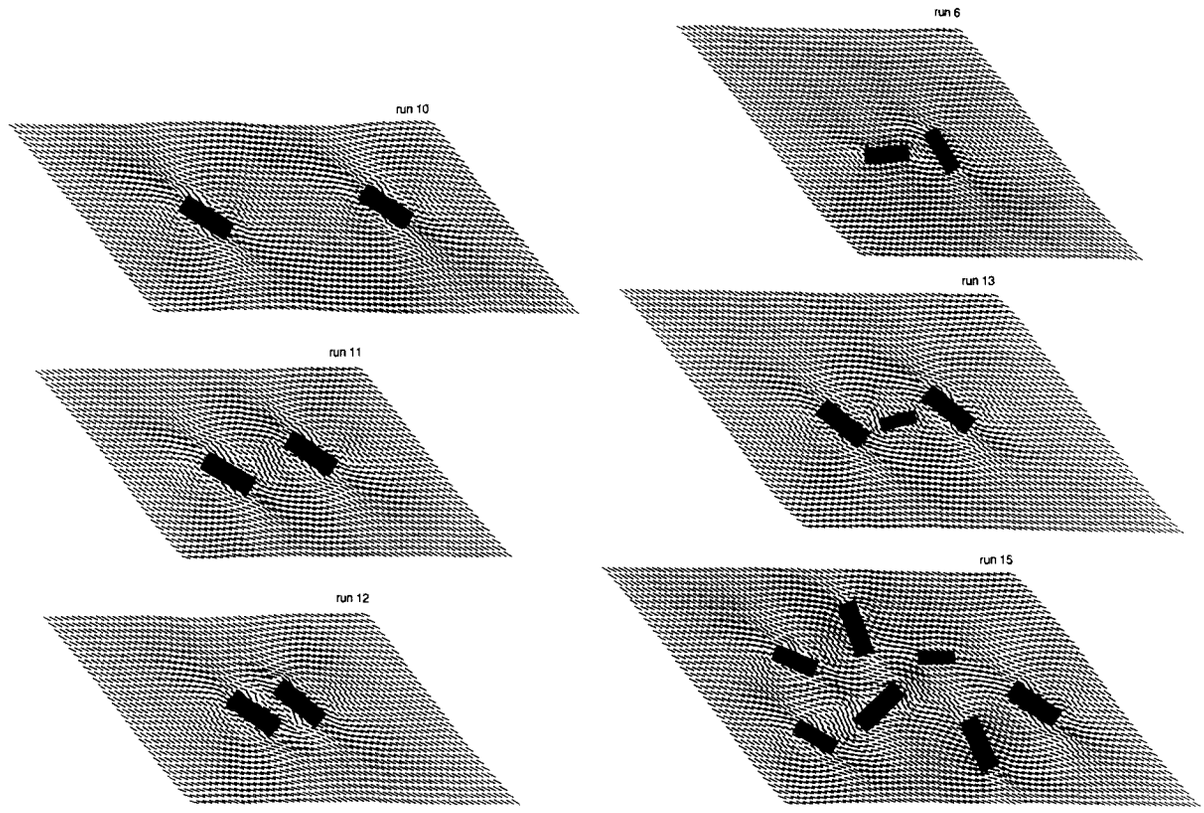

Fig. 4. Finite strain orientation pattern in runs 10, 11, 12, 6, 13 and 15. Each plotted axis is the major axis of the finite strain ellipse at a given point of the grid. Axes immediately adjacent to the particles are not significant, see text for further discussion.

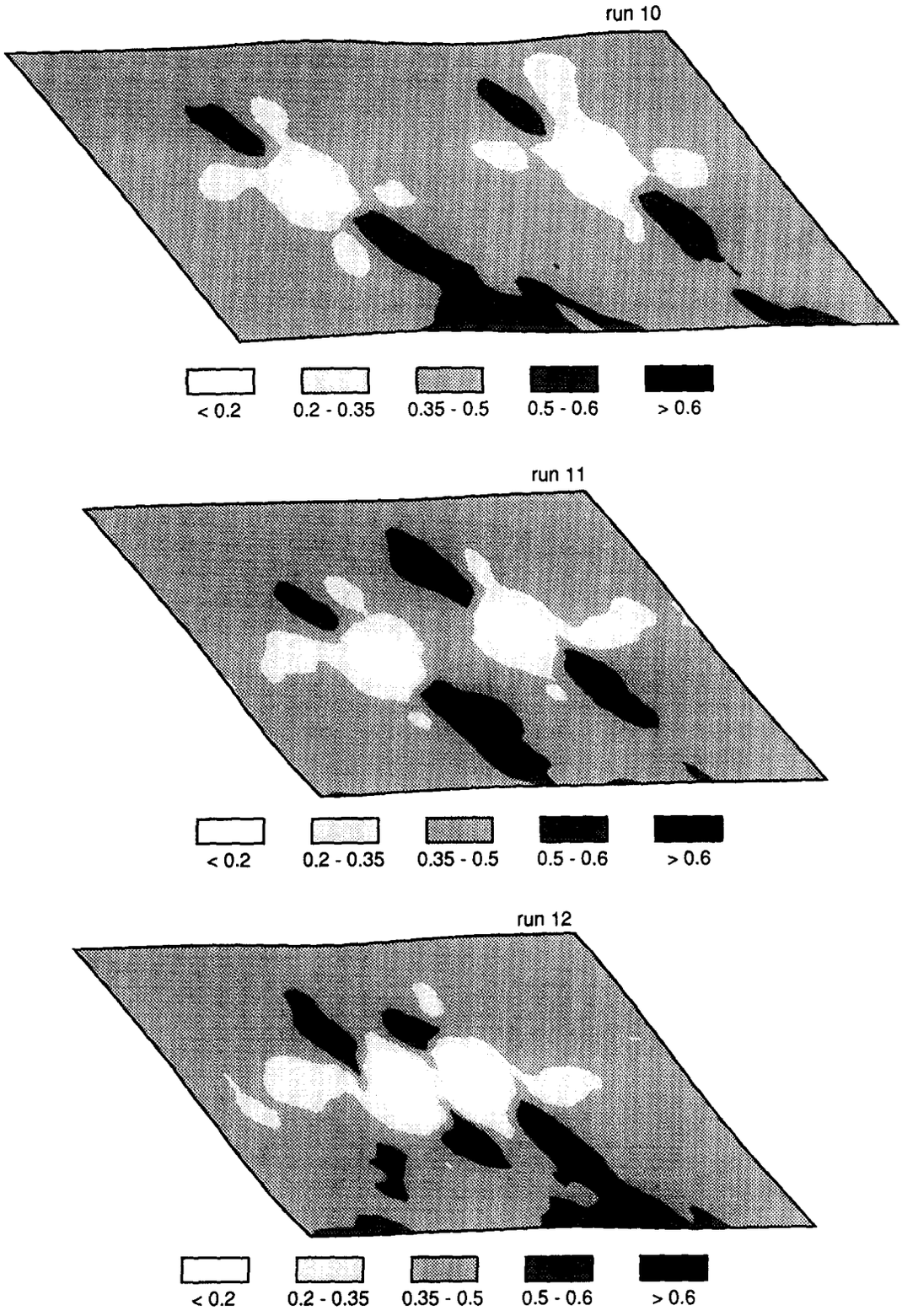

Fig. 5. Finite strain magnitude pattern in runs 10, 11, 12, 6, 13 and 15. Natural finite strain ε is calculated in each point plotted in Fig. 4; ε would be about 0.4 (sinh $\varepsilon = \gamma/2$) if the deformation had been homogeneous (see text for further discussion). Particles are not represented for better clarity, they are located in the white low-strain areas (see Figs. 2–4 for particle positions).

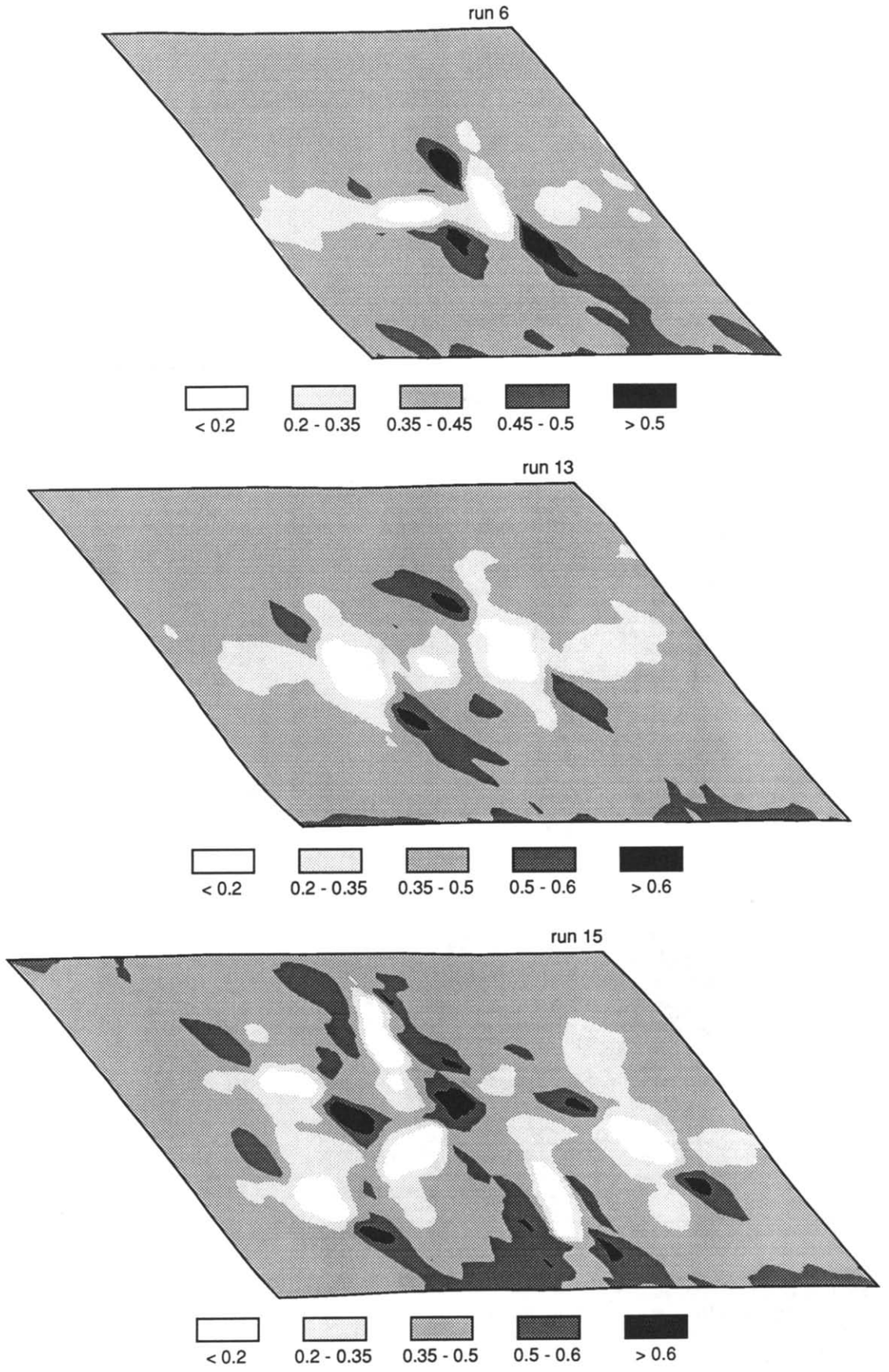

Fig. 5. *Continued.*

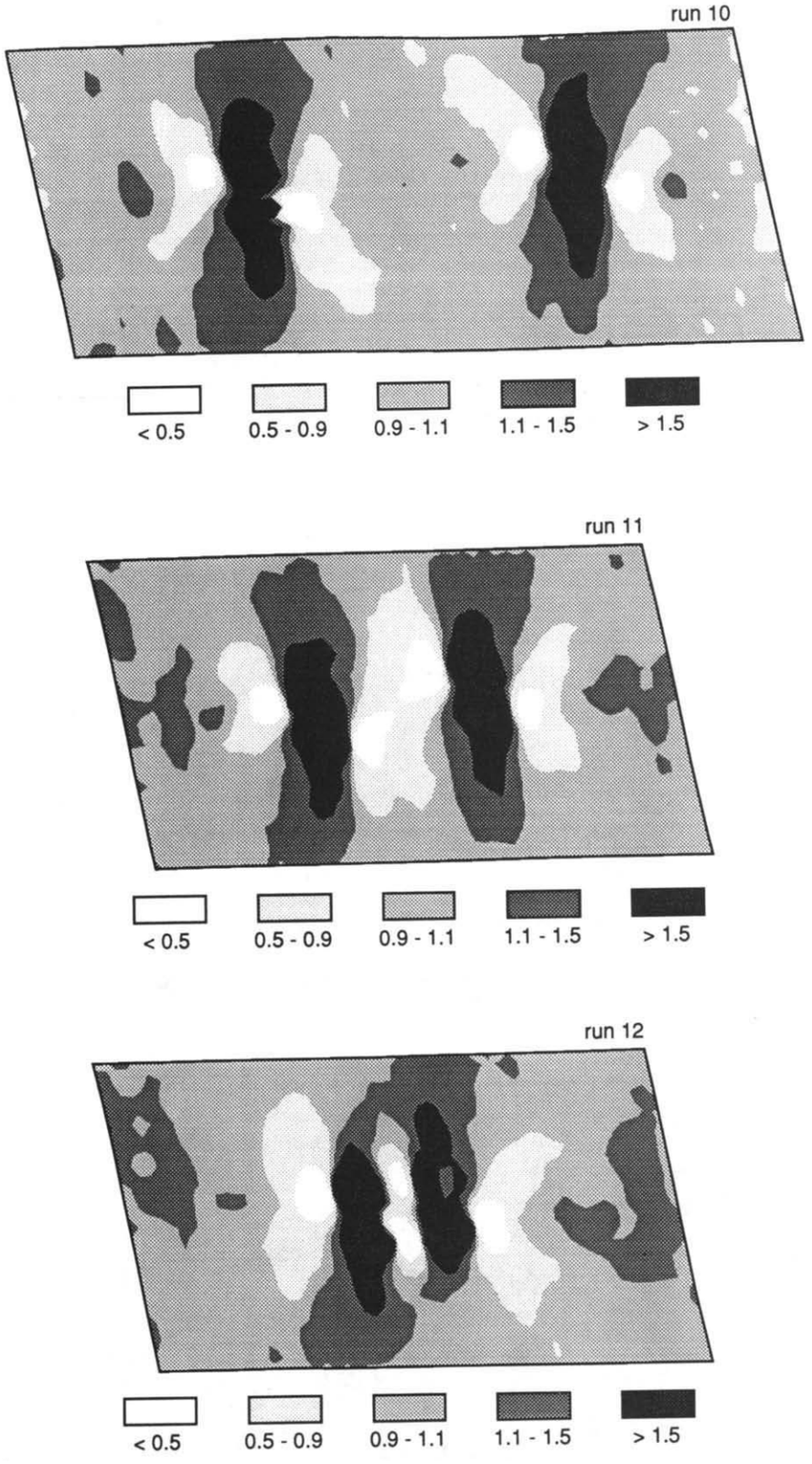

Fig. 6. Kinematic vorticity number pattern in runs 10, 11, 12, 6, 13 and 15. Kinematic vorticity number W_k is calculated in each point plotted in Fig. 4; W_k would be about 1 (simple shear) if the deformation had been homogeneous (see text for further discussion). High W_k corresponds to dark grey patterns, low W_k corresponds to light grey and white patterns. Particles are not represented for better clarity, they are located in the dark high-W_k areas (see Figs. 2–4 for particle positions).

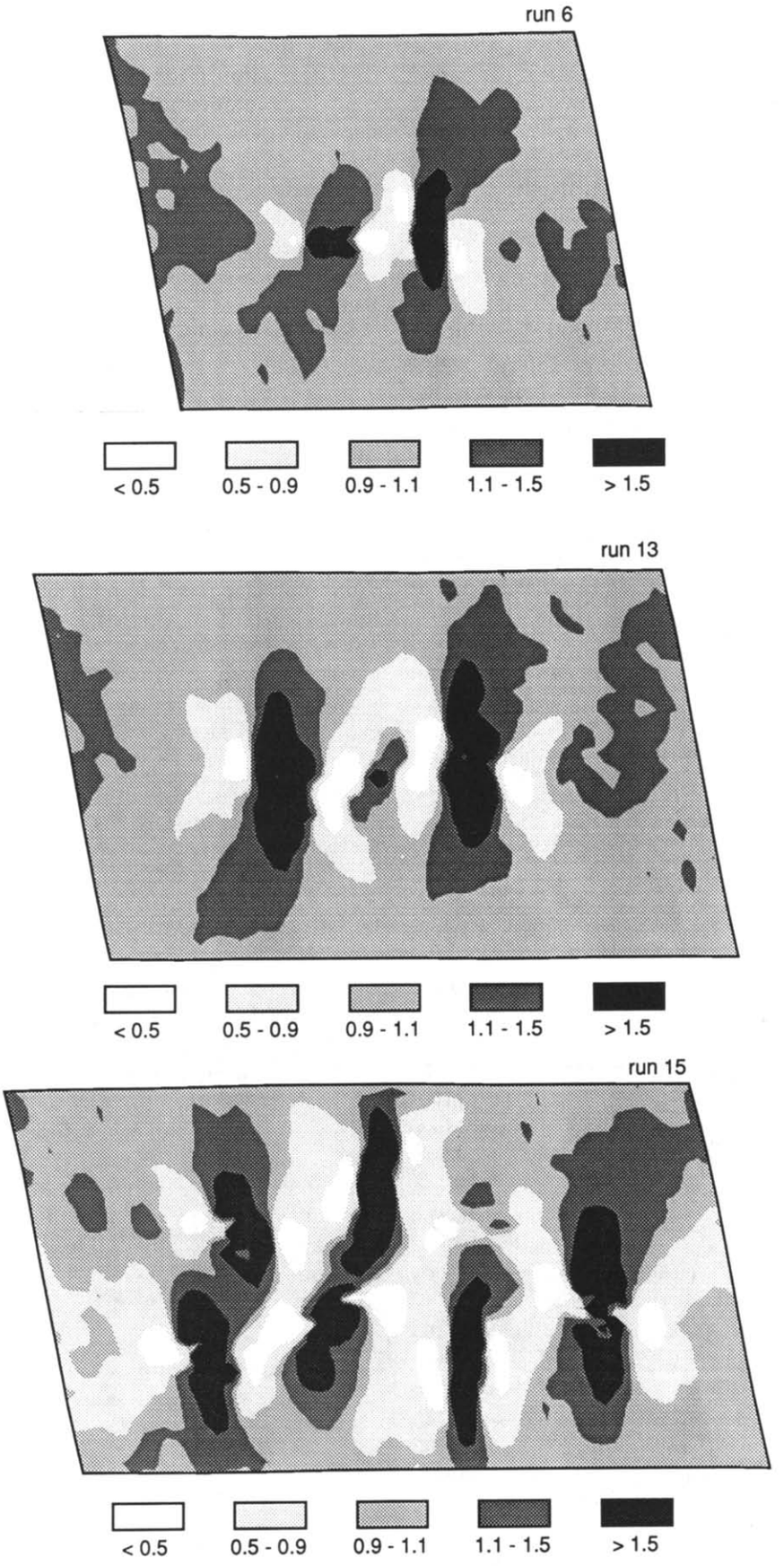

Fig. 6. *Continued.*

1986), W_k expresses the rate of rotation vs the rate of stretching for the instantaneous homogeneous deformation at the considered point. W_k ranges between 0 (coaxial flow) and ∞ (rigid-body rotation); for simple shear, $W_k = 1$. When $W_k < 1$, the flow is non-coaxial, intermediate between coaxial and simple shear, with open hyperbolic flow trajectories; when $W_k > 1$, we are in the field of the so-called pulsating flows (non-coaxial), with closed elliptical flow trajectories (Ramberg 1975, McKenzie 1979, Means *et al.* 1980, Ramsay & Huber 1983, Passchier 1986).

The kinematic vorticity number W_k has been calculated across each of the deformed grids (Mancktelow 1991); Fig. 6 shows the results on the six runs presented here, at shear strain 0.2. The background field, in white, corresponds to W_k close to 1, i.e. to flow close to simple shear. Significant perturbation around isolated particles (run 10) is then distributed as an asymmetric pattern (Fig. 6), with one zone, containing the particles, where W_k is higher than 1.1 (non-coaxial pulsating flow), and two zones where W_k is lower than 0.9 (non-coaxial flow closer to coaxial flow than simple shear). This pattern is consistent whatever the finite shear strain. At a given shear strain, the low W_k zones correspond to the zones of high finite strain. When particles are close enough for interactions to occur, the perturbation zones coalesce (run 11, 12, 6, 13 and 15). The rigid particles must then be considered in our system as local boundaries locally controlling the flow.

Effect of particle rotation on the flow in the matrix

Rotating particles behave as mobile internal boundaries within the models. The flow immediately adjacent to such internal boundaries will generally be affected by a time-dependent component of rigid-body rotation related to the time-dependent (periodic) rotation of the elongate particle.

A component of rigid-body rotation is expressed by the time-dependent rotation (sometimes called spin) of the instantaneous stretching axes in the fixed reference frame (Means *et al.* 1980, Lister & Williams 1983, Ramsay & Huber 1983, Passchier 1986), and is part of the vorticity term in W_k. The geometry of fabrics should depend only on the flow component related to the instantaneous stretching axes and not on the rigid-body rotation component. The 'degree of non-coaxiality' of the flow is then characterized by the 'internal vorticity number' (Means *et al.* 1980, Passchier 1986), in which the vorticity is given with respect to the instantaneous stretching axes and not to the fixed reference frame. Any type of flow is thus described relative to an arbitrary fixed reference frame by using this parameter (coaxial, non-coaxial or pulsating), together with the 'spin' component (spinning or non-spinning) which is the additional rigid-body rotation of the instantaneous stretching axes relative to the chosen fixed reference frame (Means *et al.* 1980, Lister & Williams 1983, Passchier 1986).

Calculating the vorticity with respect to the instantaneous stretching axes is difficult from experimental results however, because the length of the instantaneous stretching axes is so small that the error in determining their orientation is too large (particularly as high rates of rigid-body rotation are generally related to low stretching rates). The calculated absolute values for the rigid-body rotation component are, therefore, unreliable and the obtained patterns are not really consistent. For this reason, the more accurate classical 'total' vorticity number is used throughout the above discussion. It is clear, then, that it is difficult to distinguish rigid-body rotation from internal vorticity in the flow adjacent to the particles. It seems, however, that the rigid-body rotation component is not negligible.

Boundary effects

In both finite strain patterns (Fig. 5) and instantaneous deformation patterns (Fig. 6), there is some perturbation in the background fields, not related to the particles, but lying along the boundaries of the models. This boundary effect is particularly consistent in the finite strain patterns (Fig. 5), where the high strain zones around the particles tends to coalesce with high strain along the lower fixed boundary. This reveals that the background strain in the models is not perfectly homogeneous. Considering contour values close to the background strain (Fig. 7), it is difficult to distinguish a limit to the perturbation related to the particles from the perturbation related to the boundaries. The contour levels in Fig. 5 have been chosen to minimize this effect but, on the other hand, Fig. 7 shows that some information is thereby lost in Fig. 5 and not obvious in Fig. 3. If very small departures from the background finite strain are considered (Fig. 7), the particles in run 10 are close enough to produce an extensive low strain zone between them and extending beyond them, parallel to the shear plane. Flow is disturbed over a large distance away from the rigid particles, when compared to their size (at least one time the particle length).

However, boundary effect do not have critical influence on the particle rotation, because the magnitude of this effect is low compared to the total finite strain. Moreover, we compare in this study experiments with different particle configurations but identical boundary conditions, i.e. any potential boundary effect would be common to all experiments.

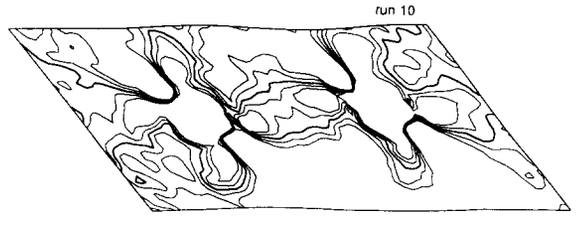

Fig. 7. Finite natural strain (ε) contours close to the background strain ($\varepsilon \approx 0.4$) in run 10. The thicker contour is $\varepsilon = 0.4$, contour interval is 0.02. ε increases towards the boundaries and diminishes toward the particle (see Figs. 2–4 for particle positions). See text for further discussion.

Particle rotation

In simple shear flow, rigid particles undergo cyclic time-dependent rotation, with a period depending on their aspect ratio (Jeffery 1922, Ramsay 1967, Gay 1968, Reed & Tryggvason 1974, Ghosh & Ramberg 1976, Fernandez *et al.* 1983, Passchier 1987), such that the orientation of a particle is, at any given time, a function of its initial orientation, its aspect ratio and the shear strain (Fig. 8). Two experiments with isolated particles have been performed (Fig. 9) for comparison with the theoretical rotation curves of Fig. 8. The rotation of the particle initially oriented perpendicular to the shear plane (run 1) fits quite well with the theoretical curve ; it rotates just slightly faster than theoretically predicted. On the other hand, the particle initially oriented parallel to the shear plane (run 9) rotates much faster than predicted. This departure from the theoretical model is most likely due to the rectangular shape of the particles in our experiments; the mathematical model assumes elliptical shapes. Such a shape effect (see also Burgers 1938, Ferguson 1979) must obviously be taken into account in the other experiments and not be mistaken for some interaction effect.

Rotation of the particles in runs 10, 11 and 12 (Figs. 2–6) is shown in Fig. 10. With the largest distance between the two particles (≈6 cm in run 10), their rotation is not disturbed; it is similar to the isolated-particle case (Fig. 9). In run 11, the distance is shorter (≈3 cm), particles rotate a little slower, but the difference from run 10 is very slight and probably of the same order of magnitude as the errors inherent in both experimental conditions and measurements. In run 12, the distance is shorter again (≈ 1 cm), shorter than particle length, and in this case, particle rotation is significantly slower, with a difference of about 5° from the theoretical curve after a shear strain of only 1.2. Figure 11 shows the result of similar experiments, but with two particles having different initial orientation (90° and 0°). Again, rotation of the particles is significantly disturbed when the distance between them is shorter than their length (≈ 1 cm in run 6, ≈3 cm in run 7).

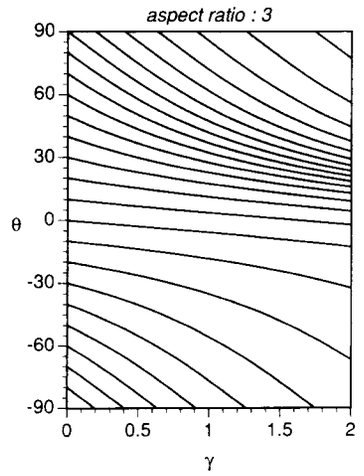

Fig. 8. Theoretical rotation curves for a rigid particle with an aspect ratio of 3 (equation in Fernandez *et al.* 1983). θ, orientation of the long axis of the particle to the shear plane; γ, shear strain.

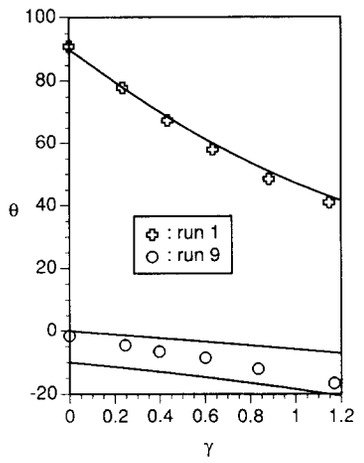

Fig. 9. Rotation of isolated particles (runs 1 and 9). Measurements from experiments (symbols) are compared to theoretical curves given in Fig. 8 (solid lines). θ, orientation to the shear plane; γ, shear strain.

In runs 13 and 15 (Figs. 2 and 4–6), particles have different initial orientation and different size. In these two experiments (Figs. 12 and 13), the smaller particle (black dots) rotates much slower than the other larger particles with similar distances between them (compare also with run 6, where the particle with the same initial orientation of 0° rotates faster). The difference from the isolated case (Fig. 9) is about 15° after a shear strain of only 1.2.

Comparison with other models

Various previous studies have already dealt with the heterogeneity of deformation around rigid inclusions, and our results concerning the deformation field are similar to what is already published. In the experiments by Ghosh (1975) and Ghosh & Ramberg (1976), strain markers in the matrix are too rare to allow visualization of the strain field (except figs. 2–4 on pp. 189–190 of Ghosh 1975). Deflection of the linear passive markers is, however, in full agreement with the asymmetric heterogeneous strain field we observe. Ghosh & Sengupta (1973) published photographs of experiments with a high concentration of stiff but deformable particles in a viscous matrix. Direct comparison with our strain fields is difficult, because it is locally largely controlled by the particles (similar situation to run 15 in Figs. 4 and 5); however, like in our experiments, strain is highly heterogeneous.

More recently, experiments have been carried out to simulate development of porphyroclast systems (Passchier & Simpson 1986, Van Den Driessche & Brun 1987). Early stages in the experiments of Van Den Driessche & Brun (1987) also show strain patterns very similar to our experiments. Strain fields are not given by Passchier & Simpson (1986); however, the geometry of the deformed grid around the particles in our experiments show similar patterns to the developing tails in their models.

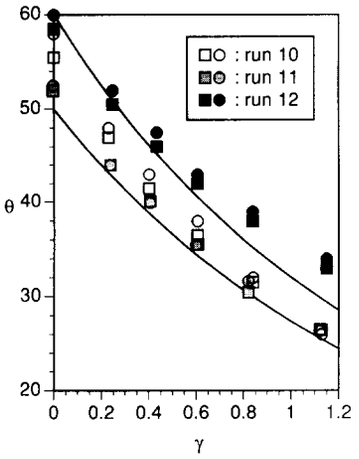

Fig. 10. Rotation of two parallel particles in runs 10, 11 and 12. The darker the symbols, the closer the particles (see text for further discussion). θ, orientation to the shear plane; γ, shear strain.

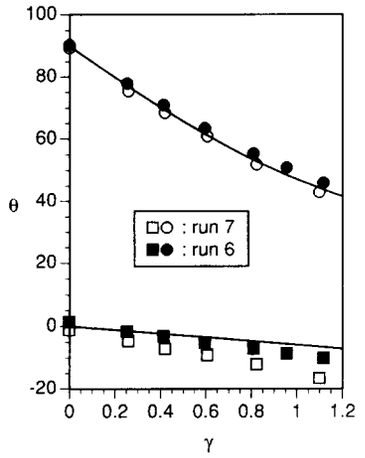

Fig. 11. Rotation of two perpendicular particles in runs 6 and 7. The darker the symbols, the closer the particles (see text for further discussion). θ, orientation to the shear plane; γ, shear strain.

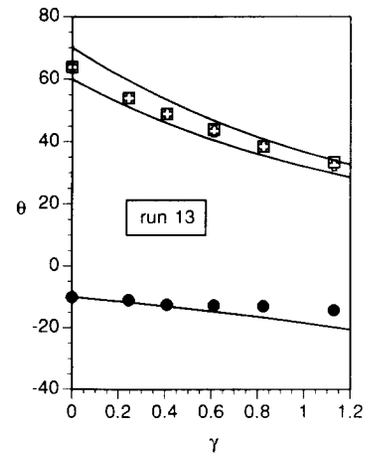

Fig. 12. Rotation of three particles in run 13. Black dots correspond to the small particle (see Figs. 2 and 4), which rotates much slower (see text for further discussion). θ, orientation to the shear plane; γ, shear strain.

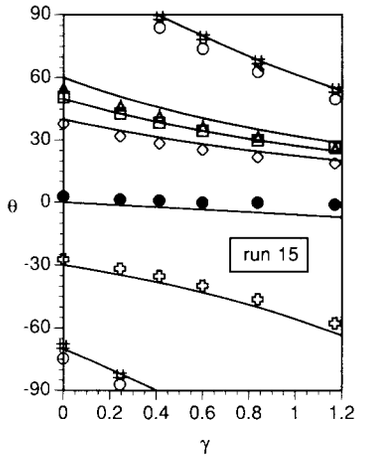

Fig. 13. Rotation of seven particles in run 15. Black dots correspond to the small particle (see Figs. 2 and 4), which rotates much slower (see text for further discussion). θ, orientation to the shear plane; γ, shear strain.

Masuda & Ando (1988) and Bjornerud (1989) present mathematical models of the deformation around rigid spheres in simple shear flow. Both models show asymmetric strain patterns similar to our experiments. Masuda & Ando (1988) also obtain a vorticity number pattern with high vorticity and low vorticity zones, but their pattern is symmetric. This difference from our results may be due to the fact that we consider elongate particles.

DISCUSSION

The results presented above are clearly specifically related to the chosen range of experimental conditions, which must be discussed before any comparison with rock structures can be attempted.

(1) The bulk maximum recorded shear strain is low ($\gamma \approx 1.2$) when compared to many natural structures. The strain field would have a different geometry at higher shear strain, with progressive passive folding around the particle, as shown for example by Van Den Driessche & Brun (1987) or by Bjornerud (1989).

(2) The matrix has a Newtonian linear viscous rheology. In a non-Newtonian flow, rotation of an isolated particle would be close to the Newtonian case, provided finite strain is not too high (Ferguson 1979). In a concentrated suspension of interacting particles, however, the flow and strain patterns may change, because of strain localization for example. Then, because of this strong local flow disturbance, the rotation of individual particles may change as well.

(3) This experimental study considers only the end-member case of rigid particles. The effect of interactions in a population of stiff but still deformable particles (Gay 1968, Ghosh & Sengupta 1973, Freeman 1987, Freeman & Lisle 1987) will obviously be different.

(4) The particle–matrix interface in these models is coherent, but this might not be always the case in nature. Odonne (1990) demonstrates the influence of movement along a fault on the adjacent deformation pattern.

First results of experiments currently performed in Zürich also demonstrate the strong influence of slip at the particle–matrix interface; the deformation pattern, as well as the particle rotation, is very different (Ildefonse & Mancktelow in preparation).

(5) Our models are only two-dimensional. Extension of quantitative results on particle rotation to three dimensions will most likely depend on additional parameters, for example the particle shape (e.g. Freeman 1985). The matrix between different rotating particles could also undergo more complex displacements outside the plane of the experiments.

With these experimental limitations in mind, our observations still have important implications on the behaviour and mechanical significance of some natural structures. The results and their implications may be summarized in the following conclusions.

CONCLUSIONS

(1) The finite strain pattern around rigid particles is strongly heterogeneous and asymmetric, with high strain areas aligned along the bulk finite strain major axis.

(2) The instantaneous deformation pattern, characterized by the kinematic vorticity number, is also heterogeneous and asymmetric. Low W_k areas (closer to coaxial flow than simple shear) correspond to the high finite strain areas, while high W_k areas (non-coaxial pulsating flow) correspond to the low finite strain ones. Such an asymmetric pattern, responsible in rocks for asymmetric structures (porphyroclast systems, deflection of foliation) now classically used as kinematic indicators (e.g. Passchier 1987, Van Den Driessche & Brun 1987, Vernon 1987) is consistently observed. The pattern of crystallographic preferred orientations in the matrix adjacent to isolated rigid objects, depending on local flow, may also be a reliable shear criterion.

(3) The heterogeneous strain patterns around rigid particles spread over a large distance when compared to the particle size and increase in extent with increasing bulk strain. The maximum extent is limited by the dimension of the shear box, but exceeds 1–2 times the length of the particle. In a concentrated suspension of rigid particles, the heterogeneous strain patterns coalesce, the overall pattern is strongly disturbed and cannot be simply related to the external boundary conditions. Particles act in the suspension as internal mobile boundaries and locally control the flow, isolating some portions of the matrix where the flow is totally different from that imposed by the external boundaries. Crystallographic preferred orientations in such portions naturally cannot reflect the bulk boundary conditions.

(4) Considering a population of equal-size particles, their rotation will be significantly disturbed when the distance between adjacent particles is shorter than their length. This means that the influence of interactions between rigid particles is probably not as dramatic as previously thought (Ildefonse & Fernandez 1988, Ildefonse *et al.* 1992) and would be significant (at least in the relatively low-strain range considered here) only for very concentrated suspensions. However, defining a critical particle density at which single particle theory seriously breaks down is still difficult. We need much more data with varying particle densities and particle size to do so.

(5) For similar distances between unequal-sized particles, the smaller particles are more affected. This result is obviously directly relevant to the analysis of sub-fabrics defined by different minerals, which has proved to be a good shear criterion (Fernandez *et al.* 1983, Benn 1989, Benn & Allard 1989). If the minerals defining the different sub-fabrics have significant different sizes (e.g. feldspars and biotites, see also Ildefonse *et al.* 1992, fig. 9), the rotation of the sub-fabric defined by the smaller particles may be very different from what is theoretically expected, and the shear criterion may therefore become unreliable.

Acknowledgements—We thank R. J. Lisle, S. K. Ghosh, B. Freeman, Sara Spencer and John Ramsay for their careful review. We are very grateful to Urs Gerber for the high quality photographic work and Emmanuel Ball for drawing Fig. 1. Professor C. J. Talbot is kindly thanked for welcoming the co-operation between Uppsala University and ETH-Zürich. Benoît Ildefonse and Neil Mancktelow were funded by Swiss National Fund grant No. 21-25258.88. Dimitrios Sokoutis was supported throughout this research by a Swedish Natural Council (N.F.R.) grant.

REFERENCES

Anczurowski, E., Cox, R. G. & Mason, S.G. 1967. The kinetics of flowing dispersions. IV. Transient orientations of cylinders. *J. Colloid Interf. Sci.* **23**, 547–562.

Benn, K. 1989. Etude cinématique des complexes plutoniques des ophiolites d'Oman et du Troodos. Unpublished thèse de doctorat, Université de Montpellier.

Benn, K. & Allard, B. 1989. Preferred mineral orientations related to magmatic flow in ophiolite layered gabbros. *J. Petrol.* **30**, 925–946.

Bjornerud, M. 1989. Mathematical model for folding of layering near rigid objects in shear deformation. *J. Struct. Geol.* **11**, 245–254.

Blanchard, J. P., Boyer, P. & Gagny, C. 1979. Un nouveau critère de sens de mise en place dans une caisse filonienne : le "pincement" des minéraux aux épontes. *Tectonophysics* **53**, 1–25.

Blumenfeld, P. & Bouchez, J. L. 1988. Shear criteria in granite and migmatite deformed in the magmatic and solid states. *J. Struct. Geol.* **10**, 361–372.

Burgers, J. M. 1938. On the motion of small particles of elongated form suspended in a viscous liquid. *Verh. K. Ned. Akad. Wet.* **16**, 113–184.

Den Tex, E. 1969. Origin of ultramafic rocks, their tectonic setting and history: a contribution to the discussion of the paper "the origin of ultramafic and ultrabasic rocks" by P. J. Willie. *Tectonophysics* **7**, 457–488.

Dixon, J. M. & Summers, J. M. 1985. Recent developments in centrifuge modelling of tectonic processes: equipment, model construction techniques and rheology of model materials. *J. Struct. Geol.* **7**, 83–102.

Ferguson, C. C. 1979. Rotations of elongate rigid particles in slow non-Newtonian flows. *Tectonophysics* **60**, 247–262.

Fernandez, A. 1988. Strain analysis from shape preferred orientation in magmatic rocks. In: *Geological Kinematics and Dynamics* (edited by Talbot, C. J.). *Bull. geol. Inst. Univ. Uppsala* **14**, 61–67.

Fernandez, A., Feybesse, J. L. & Mezure, J. F. 1983. Theoretical and experimental study of fabric developed by different shaped markers in two-dimensional simple shear. *Bull. Soc. géol. Fr.* **25**, 319–326.

Freeman, B. 1985. The motion of rigid ellipsoidal particles in slow flows. *Tectonophysics* **113**, 163–183.

Freeman, B. 1987. The behaviour of deformable ellipsoidal particles in three-dimensional shape slow flows: implications for geological strain analysis. *Tectonophysics* **132**, 297–309.

Freeman, B. & Lisle, R. J. 1987. The relationship between tectonic strain and the three-dimensional shape fabrics of pebbles in deformed conglomerates. *J. geol. Soc. Lond.* **144**, 635–639.

Gay, N. C. 1968. Pure shear and simple shear deformation of inhomogeneous viscous fluids. I—Theory. *Tectonophysics* **5**, 211–234.

Ghosh, S. K. 1975. Distortion of planar structures around rigid spherical bodies. *Tectonophysics* **28**, 185–208.

Ghosh, S. K. & Ramberg, H. 1976. Reorientation of inclusions by combination of pure shear and simple shear. *Tectonophysics* **34**, 1–70.

Ghosh, S. K. & Sengupta, S. 1973. Compression and simple shear of test models with rigid and deformable inclusions. *Tectonophysics* **17**, 133–175.

Goguel, J. 1948. Observations sur la déformation d'un calcaire métamorphique (Adamello méridional). *Bull. Soc. géol. Fr., Sér.* 5 **18**, 441–452.

Goldstein, A. G. 1988. Factors affecting the kinematic interpretation of asymmetric boudinage in shear zones. *J. Struct. Geol.* **10**, 707–715.

Hsu, T. C. 1966. A study of large deformations by matrix algebra. *J. Strain Anal.* **1**, 313–321.

Ildefonse, B. & Fernandez, A. 1988. Influence of the concentration of rigid markers in a viscous medium on the production of preferred orientations. An experimental contribution, 1. Non coaxial strain. In: *Geological Kinematics and Dynamics* (edited by Talbot, C. J.). *Bull. geol. Inst. Univ. Uppsala* **14**, 55–60.

Ildefonse, B., Lardeaux, J. M. & Caron, J. M. 1990. The behavior of shape preferred orientations in metamorphic rocks: amphiboles and jadeites from the Monte Mucrone area (Sesia-Lanzo zone, Italian Western Alps). *J. Struct. Geol.* **12**, 1005–1011.

Ildefonse, B., Launeau, P., Fernandez, A. & Bouchez, J. L. 1992. Effect of mechanical interactions on development of shape preferred orientations: a two-dimensional experimental approach. *J. Struct. Geol.* **14**, 73–83.

Jeffery, G. B. 1922. The motion of ellipsoidal particles immersed in a viscous fluid. *Proc. R. Soc. Lond.* **102**, 161–179.

Lister, G. S. & Williams, P. F. 1983. The partitioning of deformation in flowing rock masses. *Tectonophysics* **92**, 1–33.

Lloyd, G. E. & Ferguson, C. C. 1981. Boudinage structure: some new interpretations based on elastic-plastic finite element simulations. *J. Struct. Geol.* **3**, 117–128.

Malavieille, J. & Lacassin, R. 1988. 'Bone-shaped' boudins in progressive shearing. *J. Struct. Geol.* **10**, 335–345.

Mancktelow, N. S. 1991. The analysis of progressive deformation from an inscribed grid. *J. Struct. Geol.* **13**, 859–864.

Masuda, T. & Ando, S. 1988. Viscous flow around a rigid spherical body: a hydrodynamical approach. *Tectonophysics* **148**, 337–346.

McKenzie, D. 1979. Finite deformation during fluid flow. *Geophys. J. R. astr. Soc.* **58**, 689–715.

Means, W. D., Hobbs, B. E., Lister, G. S. & Williams, P. F. 1980. Vorticity and non-coaxiality in progressive deformation. *J. Struct. Geol.* **2**, 371–378.

Odonne, F. 1990. The control of deformation intensity around a fault: natural and experimental examples. *J. Struct. Geol.* **12**, 911–921.

Passchier, C. W. 1986. Flow in natural shear zones. The consequences of spining flow regimes. *Earth Planet. Sci. Lett.* **77**, 70–80.

Passchier, C. W. 1987. Stable positions of rigid objects in non-coaxial flow—a study in vorticity analysis. *J. Struct. Geol.* **9**, 679–690.

Passchier, C. W. & Simpson, C. 1986. Porphyroclast systems as kinematic indicators. *J. Struct. Geol.* **8**, 831–843.

Ramberg, H. 1975. Particle paths, displacement and progressive strain applicable to rocks. *Tectonophysics* **28**, 1–37.

Ramsay, J. G. 1967. *Folding and Fracturing of Rocks*. McGraw-Hill, New York.

Ramsay, J. G. & Huber, M. I. 1983. *The Techniques of Modern Structural Geology, Volume* 1: *Strain Analysis*. Academic Press, London.

Reed, L. J. & Tryggvason, E. 1974. Preferred orientation of rigid particles in a viscous fluid matrix deformed by pure shear and simple shear strain. *Tectonophysics* **24**, 85–98.

Sokoutis, D. 1987. Finite strain effects in experimental mullions. *J. Struct. Geol.* **9**, 233–242.

Treagus, S. H. & Sokoutis, D. 1992. Laboratory modelling of strain variation across rheological boundaries. *J. Struct. Geol.* **14**, 405–424.

Truesdell, C. 1953. Two measures of vorticity. *J. Rational Mech. Anal.* **2**, 173–217.

Van Den Driessche, J. & Brun, J. P. 1987. Rolling structures at large shear strain. *J. Struct. Geol.* **9**, 691–704.

Vernon, R. H. 1987. A microstructural indicator of shear sense in volcanic rocks and its relationship to porphyroblast rotation in metamorphic rocks. *J. Geol.* **95**, 127–133.